University of Groningen

In EXOG-depleted cardiomyocytes cell death is marked by a decreased mitochondrial reserve capacity of the electron transport chain

Tigchelaar, Wardit; De Jong, Anne Margreet; van Gilst, Wiek H.; de Boer, Rudolf; Sillje, Herman

IMPORTANT NOTE: You are advised to consult the publisher's version (publisher's PDF) if you wish to cite from it. Please check the document version below.

Document Version
Publisher's PDF, also known as Version of record

Publication date:
2016

Link to publication in University of Groningen/UMCG research database

Primary Research

In EXOG-depleted cardiomyocytes cell death is marked by a decreased mitochondrial reserve capacity of the electron transport chain

Wardit Tigchelaar, Anne Margreet De Jong, Wiek H. van Gilst, Rudolf A. De Boer and Herman H.W. Silljé*

Depletion of mitochondrial endo/exonuclease G-like (EXOG) in cultured neonatal cardiomyocytes stimulates mitochondrial oxygen consumption rate (OCR) and induces hypertrophy via reactive oxygen species (ROS). Here, we show that neurohormonal stress triggers cell death in endo/exonuclease G-like-depleted cells, and this is marked by a decrease in mitochondrial reserve capacity. Neurohormonal stimulation with phenylephrine (PE) did not have an additive effect on the hypertrophic response induced by endo/exonuclease G-like depletion. Interestingly, PE-induced atrial natriuretic peptide (ANP) gene expression was completely abolished in endo/exonuclease G-like-depleted cells, suggesting a reverse signaling function of endo/exonuclease G-like. Endo/exonuclease G-like depletion initially resulted in increased mitochondrial OCR, but this declined upon PE stimulation. In particular, the reserve capacity of the mitochondrial respiratory chain and maximal respiration were the first indicators of perturbations in mitochondrial respiration, and these marked the subsequent decline in mitochondrial function. Although pathological stimulation accelerated these processes, prolonged EXOG depletion also resulted in a decline in mitochondrial function. At early stages of endo/exonuclease G-like depletion, mitochondrial ROS production was increased, but this did not affect mitochondrial DNA (mtDNA) integrity. After prolonged depletion, ROS levels returned to control values, despite hyperpolariza-

tion of the mitochondrial membrane. The mitochondrial dysfunction finally resulted in cell death, which appears to be mainly a form of necrosis. In conclusion, endo/exonuclease G-like plays an essential role in cardiomyocyte physiology. Loss of endo/exonuclease G-like results in diminished adaptation to pathological stress. The decline in maximal respiration and reserve capacity is the first sign of mitochondrial dysfunction that determines subsequent cell death.

Introduction

Cardiac hypertrophy is the cellular response to increased ventricular wall stress and can be induced by a variety of pathological stimuli like hypertension, valvular disease and myocardial infarction, and also by physiological stimuli including endurance exercise and pregnancy [1–3]. Hypertrophy is defined by an increase in cardiomyocyte size and is accompanied by enhanced protein synthesis and changes in sarcomere organization [4]. This response is initially an adaptive mechanism of the heart to cope with this increased wall stress. However, hypertrophy induced by sustained pathological stimulation, like neurohormonal stimulation, is not reversible and may become maladaptive. Under these conditions, the initially adaptive response of compensated hypertrophy may advance into decompensated hypertrophy and subsequently result in heart failure [5].

Hypertrophy is also accompanied by metabolic alterations and changes in mitochondrial energy production in the muscle cells, including altered substrate utilization [6, 7]. It is more and more recognized that mitochondrial dysfunction is an important event in the development of heart failure [8]. This is plausible, as the heart is the most energy-consuming organ in the body and is largely dependent on mitochondrial metabolism to generate energy in the form of ATP to sustain proper cardiac function [9]. Although the basic aspects of mitochondrial metabolism and energetics, including electron transfer and ATP production, are well established, relatively little is

known about the mechanisms and pathways leading to mitochondrial energetic dysfunction in hypertrophy [10]. In heart failure, the mitochondria in cardiomyocytes appear to be intact but functionally impaired [8]. This provides opportunities for therapeutic interventions, but it will require a better understanding of genes and processes that affect mitochondrial function.

Besides the role of mitochondria in providing energy, they also generate reactive oxygen species (ROS). Under physiological conditions, minor amounts of ROS are produced that can be detoxified or act as signaling molecules [11]. Changes in mitochondrial function can result in increased production of ROS, triggering signal transduction pathways and/or resulting in cellular damage [11]. In addition, mitochondria play a central role in cell death mechanisms, including apoptosis and regulated necrosis [12, 13]. Thus, mitochondria have a key position in regulating and maintaining cellular functions.

Recently, we demonstrated that mitochondrial endo/exonuclease G-like (EXOG) modulates mitochondrial respiration and hypertrophy in cardiomyocytes [14]. Interestingly, the EXOG-containing locus was previously identified in a genome-wide association study on QRS duration, which is a risk factor for heart failure [15]. Hence, we hypothesized that perturbed EXOG function may affect human heart function. We reported that in EXOG-depleted cardiomyocytes, mitochondrial respiration is strongly enhanced and a concomitant increase in ROS has been observed. These increased ROS levels triggered cell growth, resulting in a hypertrophic phenotype [14]. In clear contrast, in EXOG-depleted cancer cell lines, mitochondrial DNA (mtDNA) damage was reported, resulting in diminished mitochondrial respiration [16]. Moreover, in myoblasts, but not in myotubes, increased EXOG levels were protective against oxidative stress [17]. Thus, it appears that EXOG affects mitochondrial function in different ways depending on the cell type and the cellular environment, including cellular stress. The role of EXOG under cardiac stress and whether EXOG function is essential under these conditions are not known. Cultured neonatal rat ventricular cardiomyocytes (NRVCs) are an excellent in vitro model to study cardiac stress conditions that mimic pathological hypertrophy, like adrenergic stimulation. So, in this study, we investigated the role of EXOG under conditions of pathological cardiac stress in these non-proliferative cardiomyocytes. To this aim, we stimulated EXOG-depleted cardiomyocytes with phenylephrine (PE) and evaluated mitochondrial function, including mitochondrial respiration and cell death.

Materials and methods

Isolation and culturing of primary cardiomyocytes

The use of animals for this study was in accordance with the National Institutes of Health (NIH) Guide for the Care and Use of Laboratory Animals. The study was submitted to and approved by the Committee for Animal Experiments of the University of Groningen. Primary NRVCs were isolated from neonatal rats of 1–3 days old, as previously described [18, 19]. NRVCs were grown in Dulbecco's modified Eagle's medium (DMEM) supplemented with 5% fetal calf serum (FCS) and penicillin-streptomycin ($100 \, U \cdot mL^{-1}$ to $100 \, \mu g \cdot mL^{-1}$), and during the first day, 0.1 mM BrdU was included to prevent proliferation of fibroblasts. NRVCs were infected with recombinant adenoviral particles [multiplicity of infection (MOI) 50] 24 hours after isolation and serum starved in DMEM with penicillin-streptomycin ($100 \, U \cdot mL^{-1}$ to $100 \, \mu g \cdot mL^{-1}$) the next day. At this MOI, nearly all cardiomyocytes become infected and express green fluorescent protein (GFP), which is co-expressed with the short hairpin RNAs (shRNA). Recombinant adenovirus expressing shRNAs targeting EXOG or control shRNA virus (with a non-specific sequence) have been described before [14]. Cells were infected with virus for 72 or 144 hours. Stimulation of cells with 50 μM PE was carried out after 24 hours of starvation, resulting in 24 or 96 hours of stimulation. Inhibitors Z-VAD fmk (carbobenzoxy-valyl-alanyl-aspartyl-[O-methyl]-fluoromethyl ketone) (20 μM) and MitoTEMPO (1 μM) were added at the same time of infection. All media and supplements were purchased from Sigma-Aldrich Chemie B.V., Zwijndrecht, the Netherlands.

Hypertrophy measurements

Protein synthesis was measured via the incorporation of radioactive labeled ^{3}H-leucine, as described before [20].

For cell size measurements, NRVCs were grown on cover slips coated with laminin (Millipore, Amsterdam, the Netherlands) and cultured as described earlier. After fixation for 10 minutes with paraformaldehyde, cells were permeabilized with 0.5% Triton X. Cells were incubated with monoclonal anti-α-actinin antibody (Sigma-Aldrich Chemie B.V.) in 1% bovine serum albumin (BSA)/phosphate-buffered saline (PBS) for 1 hour at room temperature (RT). Cells were washed and incubated for another hour with Alexa-555 secondary antibody (Invitrogen Life Technologies Europe B.V., Bleiswijk, the Netherlands). Cover slips were mounted with mounting medium containing DAPI for counterstaining of the nuclei, and slides were imaged using a TissueFAXS (Axio Observer Z1 microscope, Carl Zeiss, Jena, Germany), and cell size was determined by TISSUEQUEST fluorescence analysis software.

Quantitative real-time polymerase chain reaction

Total RNA was isolated using a NucleoSpin RNA II kit (Bioké, Leiden, the Netherlands), and cDNA was synthesized using QuantiTect Reverse Transcription Kit (Qiagen, Venlo, the Netherlands) following manufacturer's instructions. Relative gene expression was determined by quantitative real-time polymerase chain reaction (qRT-PCR) on the Bio-Rad CFX384 real-time system (Bio-Rad, Veenendaal, the Netherlands) using ABsolute qPCR SYBR Green Mix (Thermo Scientific, Landsmeer, the Netherlands). NPPA [atrial natriuretic peptide (ANP)] gene expression was corrected for reference gene values (36B4) and expressed relative to the control group. Primer sequences included ANP forward atgggctccttctccatcac, ANP reverse tctaccggcatcttctcctc, 36B4 forward gttgcctcagtgcctcactc and 36B4 reverse gcagccgcaaatgcagatgg.

Seahorse mitochondrial flux analyses

To determine oxygen consumption rate (OCR) in cardiomyocytes, a Seahorse metabolic flux analyzer (Seahorse Bioscience, North Billerica, MA, USA) was used as previously described [21].

Neonatal cardiomyocytes were seeded at a density of 100,000 cells per well in special Seahorse 24-well plates. Cells were adenoviral infected and treated as described earlier. One hour before initiation of the Seahorse measurements, medium was replaced with XF medium supplemented with 10 mM glucose and incubated for 1 hour in a CO_2-free 37 °C incubator. Basal respiration of cells was measured, followed by injection of oligomycin (ATP synthase inhibitor) (1 μM) to measure ATP-linked OCR. The uncoupler carbonyl cyanide 4-(trifluoromethoxy)phenylhydrazone (FCCP) (0.5 μM) was used to determine maximal respiration. Finally, rotenone (1 μM) and antimycin A (1 μM), inhibiting complexes I and III, respectively, were injected to determine the non-mitochondrial respiration. In each plate, the same treatment was performed in triplicate or quadruplicate. OCR was corrected for the amount of total protein in each well.

DNA damage

Total DNA including mtDNA was extracted from cells using the DNeasy Blood & Tissue Kit (Qiagen), and DNA purity and quantity were determined by spectroscopic analysis. The isolated DNA showed high purity ($A_{260}/A_{280} > 1.8$). The D-loop mitochondrial genomic region was amplified by PCR because this part of the mitochondrial genome is described to be the most susceptible to DNA damage [22]. This was performed with a semi-long-run qRT-PCR as described before [14, 22].

Determination of mitochondrial membrane potential

Mitochondrial membrane potential ($\Delta\Psi m$) was assessed by tetramethylrhodamine ethyl ester (TMRE), as described before [21]. In brief, cells were seeded at a density of 40,000 cells per well in a black 96-well plate and cultured as described earlier. TMRE (100 nM) was added and incubated for 20 minutes at 37 °C. Cells were subsequently washed with 0.2% BSA in PBS, and fluorescence was measured at an excitation of 549 nm and emission of 575 nm with a SynergyH4 Hybrid Reader (BioTek, Winooski, VT, USA). As a control, FCCP (1 μM) was used to eliminate mitochondrial membrane potential. Each experiment was measured in quadruplicate.

Mitochondrial ROS

Mitochondrial ROS production was determined using MitoSOX red mitochondrial superoxide indicator (Molecular Life Technologies Europe B.V., Bleiswijk, the Netherlands) as described before [21]. Briefly, cells were plated in 96-well plates and cultured as described earlier. Cells were subsequently incubated with MitoSOX (2.5 μM) in Krebs-Ringer-Phosphate-HEPES (KRPH) buffer (20 mM HEPES, 5 mM KH_2PO_4, 1 mM $MgSO_4$, 1 mM $CaCl_2$, 136 mM NaCl, 4.7 mM KCl pH 7.4) for 10 minutes at 37 °C and thereafter washed three times with the same buffer. Fluorescence was measured using excitation/emission maxima of 510/580 nm with a SynergyH4 Hybrid Reader (BioTek).

Microscopic analysis of cell death

For counting dead cells, NRVCs were grown and treated as described earlier. Cells were incubated with Hoechst 33342 (2 μg·μL^{-1}) and propidium iodide (PI; 3 μg·μL^{-1}) and imaged using Leica DM6000. PI-positive dead cells relative to total cells (Hoechst positive) were determined per field.

For counting apoptotic cells, NRVCs were fixed for 10 minutes with 4% paraformaldehyde at 4 °C, followed by permeabilization with 0.5% Triton X for 5 minutes. Cells were incubated with monoclonal anti-cleaved caspase 3 antibody (Sigma-Aldrich Chemie B.V.) in 1% BSA, 2% normal goat serum and 0.1% Tween in PBS for 1 hour at RT. Cells were washed with PBS and incubated for another hour with a goat anti-mouse Fluorescein isothiocyanate (FITC) secondary antibody (Santa-Cruz Biotechnology, Heidelberg, Germany). Cover slips were mounted with mounting medium containing DAPI (Vector Laboratories, Burlingame, CA, USA) for counterstaining of the nuclei. Slides were imaged using Leica DM6000, and cleaved caspase-positive cells were counted, relative to the total amount of cells per field.

Lactate dehydrogenase activity

Lactate dehydrogenase (LDH) is a cytosolic enzyme that is an indicator of cellular toxicity and was monitored by the LDH release assay. LDH activity was determined in cell culture medium using the Roche International Federation of Clinical Chemistry (IFCC) liquid assay on the modular analysis according to the manufacturer's instructions (Roche, Mannheim, Germany).

Statistical analysis

All values are presented as means ± standard errors of the mean (SEM). Independent-samples t-test was performed to compare the difference between two groups. One-way analysis of variance (ANOVA) with post hoc Bonferroni test was used to compare the difference between multiple groups. $p < 0.05$ was considered to be significant. SPSS software (PASW Statistics 22, IBM Corporation, Armonk, NY, USA) was used for the statistical analyses.

Results

EXOG depletion and PE induce hypertrophy in neonatal cardiomyocytes

We have recently shown that EXOG depletion stimulates mitochondrial respiration and causes ROS-mediated cardiomyocyte hypertrophy [14]. This is surprising because EXOG is known as an mtDNA repair enzyme and protects the mitochondrial genome from oxidative stress in a proliferating myoblast cell line [16, 17]. We therefore decided to investigate whether EXOG would have more critical effects in cardiomyocytes under stress conditions by neurohormonal stimulation with PE. We first assessed hypertrophy development in EXOG-depleted NRVCs in the presence and absence of PE. As shown in Fig. 1, both EXOG depletion and PE stimulation generated a hypertrophic response indicated by increased protein synthesis (Fig. 1A) and cell size (Fig. 1B). Although in PE the stimulated EXOG-depleted cells protein synthesis appeared somewhat higher than in PE-stimulated control cells, this difference was not significant (Fig. 1A). The increase in cell size in EXOG-depleted cells, as determined using microscopy, was similar to that of PE stimulation in control cells (Fig. 1B). EXOG depletion did not significantly augment the PE-induced hypertrophic response. The mRNA expression of the established pathological hypertrophic marker ANP was also determined. Stimulation of NRVC with PE significantly induced ANP expression, whereas
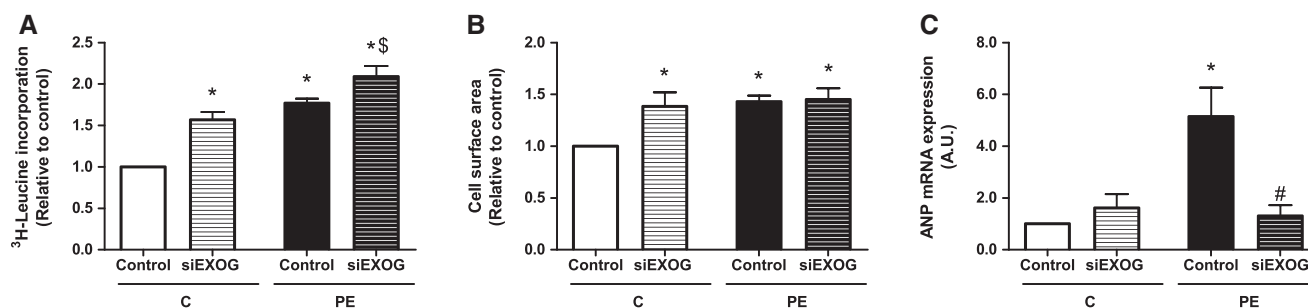
Figure 1. Effects of EXOG depletion on PE-induced hypertrophic responses. Neonatal rat ventricular cardiomyocytes were infected with control or EXOG-specific shRNA expressing adenovirus for 72 hours and stimulated with or without PE for 24 hours. EXOG silencing is indicated as siEXOG. **A**: Protein synthesis was determined by leucine incorporation ($N = 12$). **B**: Cell surface area was measured using a TissueFAXS ($N = 9$–6). **C**: Gene expression of the hypertrophic marker ANP was determined by RT-PCR ($N = 7$–11). All graphs depict means and SEM, and a one-way ANOVA with post hoc Bonferroni test was used to compare the difference between multiple groups. $*p < 0.05$ as compared with control; $\#p < 0.05$ as compared with control with PE; $\$p < 0.05$ as compared with siEXOG.

EXOG depletion had no effect on ANP expression. Surprisingly, EXOG depletion fully prevented PE-mediated ANP expression (Fig. 1C). Thus, EXOG appears to be modulating pathological ANP gene expression under these conditions.

EXOG depletion reduces maximal respiration and reserve capacity in PE-stimulated cells

Stimulation of NRVC with PE and depletion of EXOG both stimulate mitochondrial respiration in NRVCs [14, 21], but whether these effects are interdependent is not known. Here, we investigated the combined response on metabolic respiration of NRVCs to stimulation with PE and 72 hours of EXOG depletion. EXOG depletion increased mitochondrial respiration and ATP-linked respiration (Fig. 2A, B). Although not significant, an increase in maximal respiration, induced with the uncoupler FCCP, and the reserve capacity, which is the difference between maximal respiration and mitochondrial respiration, was observed (Fig. 2A, B). Also, PE stimulation resulted in an increase in respiration as compared with control cells (Fig. 2C). EXOG depletion did not show an additive effect on mitochondrial respiration in the presence of PE. In contrast, EXOG depletion resulted in a strong attenuation of PE-induced maximal respiration and reserve capacity (Fig. 2C, D). Despite this attenuation, ATP-linked respiration was maintained (Fig. 2D), and these cells still showed a normal hypertrophic response (Fig. 1A and B), indicating viable cells. Thus, stimulation with PE of EXOG-depleted cells does not have additive effects on mitochondrial respiration, and the diminished increase in maximal respiration and reserve capacity may suggest detrimental rather than positive effects of EXOG depletion under these pathological conditions.

### Mitochondrial respiration is decreased upon prolonged PE stimulation of depleted cells

The reserve capacity is believed to be an important determinant in coping with cellular stress [23, 24]. Because EXOG-depleted cells showed a decreased reserve capacity after stimulation with PE, this may provide a first indication that EXOG-depleted cells are unable to adapt properly to changes induced by this pathological stress factor. As shown in Supporting Information Figure 1, EXOG depletion remained

constant for at least 144 hours, and we therefore decided to investigate mitochondrial function at later time points after EXOG depletion. In Fig. 3A and B, it is shown that mitochondrial OCR is strongly declined in cells that are EXOG depleted for 144 hours and stimulated with PE, as compared with control PE-stimulated cells. Also, maximal respiration, reserve capacity and ATP-linked OCR were strongly declined, indicating that mitochondrial respiration was strongly hampered at this time point. To exclude the effect of differences in cell number and cell size, the OCR values were corrected for amount of protein per well. To investigate whether this was not solely an effect of EXOG depletion, OCR of EXOG-depleted cells at the same moment was measured. Although these cells also showed a decline in cellular respiration, mitochondrial-specific OCR and ATP-linked OCR were still comparable with the control cells, but reserve capacity and maximal respiration were lower, albeit not significantly (Fig. 3C and D). Thus, prolonged EXOG depletion resulted in mitochondrial dysfunction, and this was strongly exacerbated by stimulation with PE.

Depletion of EXOG did not result in mtDNA damage but increased mitochondrial membrane potential

As the function of EXOG has been linked to DNA repair mechanisms [16], we investigated whether the decline in OCR after PE stimulation of prolonged EXOG-depleted NRVCs could be explained by an increase in mtDNA damage. We performed a semi-long-run PCR to detect mtDNA damage lesion. mtDNA damage was not increased between the different conditions, indicating that the decline in mitochondrial function was not a result of mtDNA damage (Fig. 4A and B). As shown, before, EXOG depletion did not also affect the mtDNA/nDNA ratio (Supporting Information Figure 2).

Loss of the proton motive force, the pH gradient and membrane potential will result in the loss of ATP synthesis via oxidative phosphorylation and result in cell death. Therefore, we investigated this potential using TMRE fluorescence. After 72 hours of EXOG depletion, we did not observe any significant changes in membrane potential between EXOG-depleted cells, PE-stimulated cells and the combination of both (Fig. 4C). After prolonged depletion of EXOG, the membrane potential was even increased both in the presence and in the absence of PE (Fig. 4D).
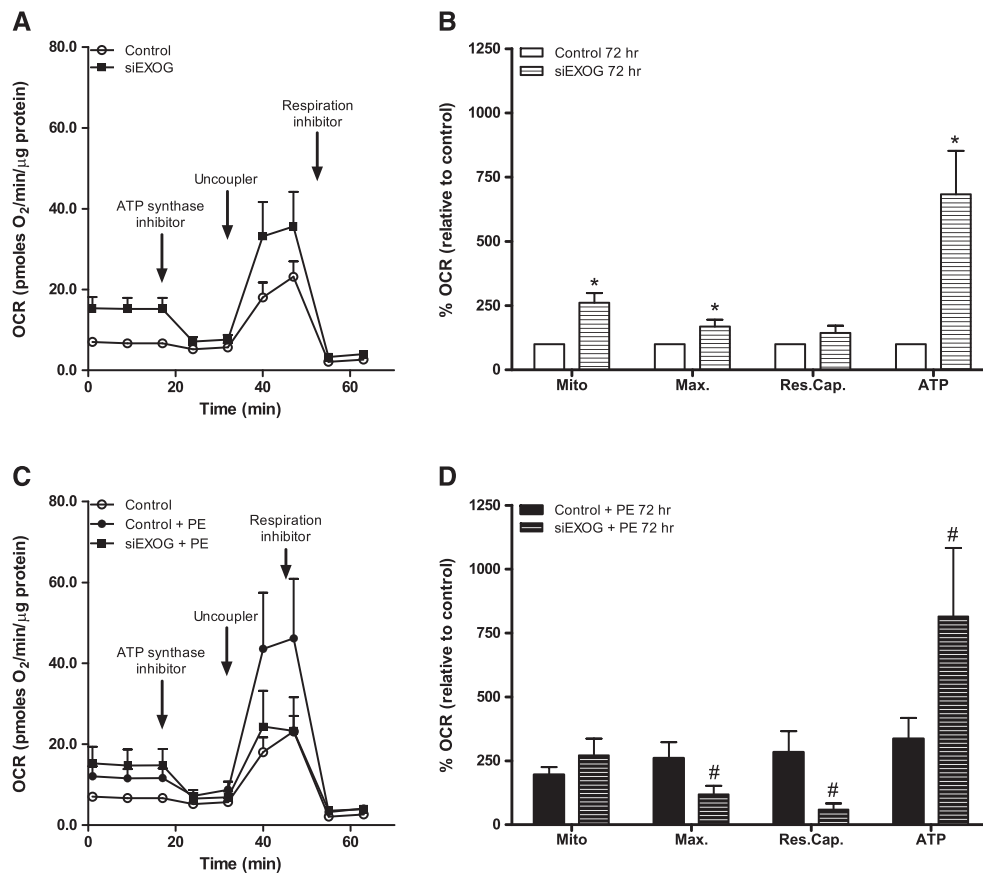
Figure 2. Effect of EXOG depletion on cellular oxygen consumption rate (OCR). OCR was measured in a Seahorse XF24 extracellular flux analyzer in NRVC. Glucose (10 mM) was used as a substrate. **A**: Total OCR was measured in cells infected for 72 hours with control or siEXOG adenovirus; addition of oligomycin (ATP synthase inhibitor), FCCP and antimycin A and rotenone (respiration inhibitor) is indicated. **B**: Quantification of mitochondrial OCR (Mito), maximal OCR (Max.), reserve capacity (Res.Cap.) and ATP-linked OCR (ATP) of the conditions shown in **A** relative to mitochondrial OCR of control cells. Mitochondrial OCR is the difference between the basal respiration and the OCR after addition of respiration inhibitor; maximal respiration is defined as the OCR induced after FCCP injection; reserve capacity is calculated as the difference between maximal respiration and basal respiration; and the ATP-linked OCR is defined as oligomycin-sensitive OCR ($N = 6$–9). **C**: Total OCR measurements, comparable with those shown in **A**, except that cells were also stimulated with PE for 24 hours. **D**: Quantification of the graph shown in **C**, relative to mitochondrial OCR of control cells. OCR was corrected for total protein levels in each well, and all measurements were performed at least in triplicates. All graphs depict means and SEM; independent-samples t-test was performed to compare the difference between both groups. *$p < 0.05$ as compared with control; #$p < 0.05$ as compared with control with PE. EXOG silencing is indicated as siEXOG.

We wondered whether this increase in mitochondrial membrane potential was associated with increased ROS production. As shown in Fig. 4E, EXOG depletion increased ROS production, and this response was exacerbated after stimulation with PE. However, after 144 hours of EXOG depletion, this increased ROS production was diminished (Fig. 4F). Thus, although initially an increased ROS production is observed, most likely as a result of increased flux, this high ROS production is not maintained.

Prolonged depletion of EXOG causes cell death, which is enhanced by pathological stimulation

As mitochondrial dysfunction is apparent, we next investigated if prolonged EXOG depletion induced cell death. We microscopically determined cell numbers and observed no obvious change within the first 72 hours of depletion, also not in the presence of PE (Fig. 5A and B). However, prolonged depletion of EXOG significantly decreased cell numbers. Again, this effect

was strongly exacerbated in PE-stimulated EXOG-depleted cells (Fig. 5A and C). Under these conditions, we observed a higher number of fibroblasts, which was merely a result of decreased numbers of cardiomyocytes.

To corroborate this finding, we also stained the cells with PI, which stains nuclei of dead cells. Hoechst was used as a counterstain, which stains nuclei of all cells. As expected, no increase in PI-positive cells was observed after 72 hours of EXOG depletion, with or without stimulation with PE (Fig. 5D). An increase in PI-positive cells was observed after 144 hours of EXOG depletion and was more elevated with PE (Fig. 5E).

Prolonged depletion of EXOG results in cell death with features of necrosis

As PI can stain the nuclei of both late apoptotic and necrotic cells, we next investigated whether programmed cell death via apoptosis occurred. NRVCs were stained with an antibody
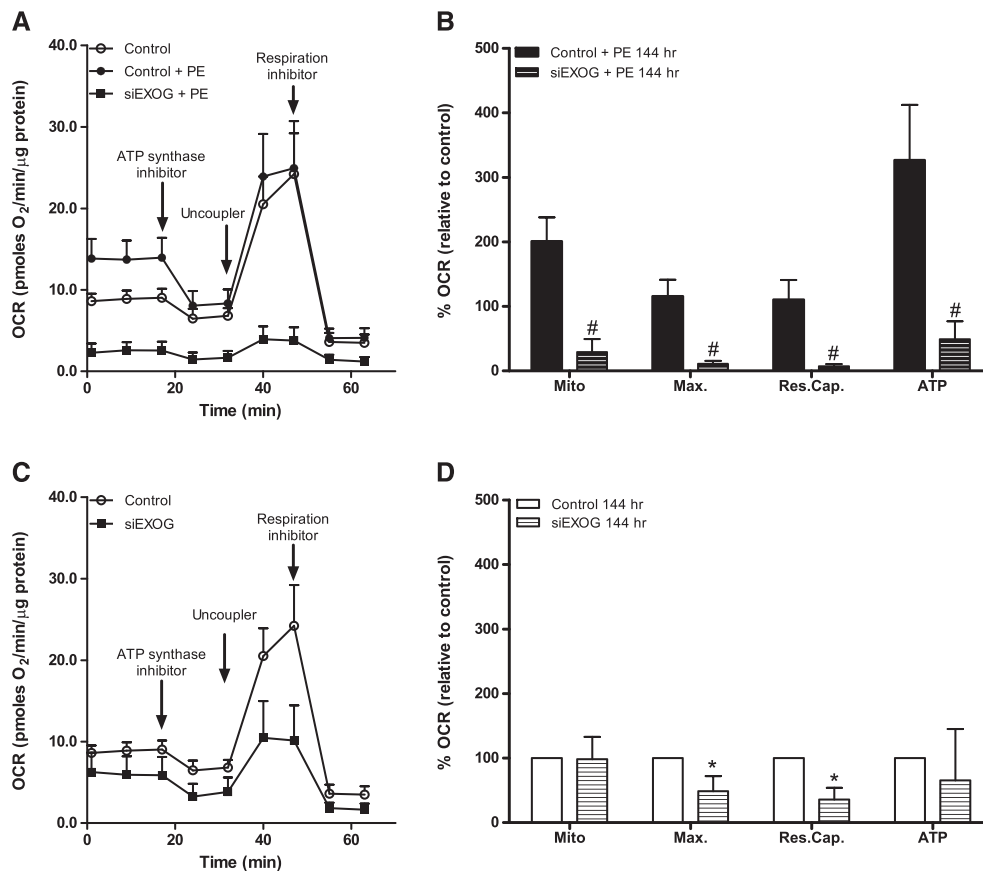
Figure 3. Effect of prolonged EXOG depletion on cellular oxygen consumption rate (OCR). OCR was measured using the same protocol as used in Fig. 2. **A**: Total OCR was measured in cells infected for 144 hours, with control or siEXOG virus stimulated with PE for 96 hours ($N = 6$). **B**: Quantification of mitochondrial OCR (Mito), maximal OCR (Max.), reserve capacity (Res.Cap.) and ATP-linked OCR (ATP) of the conditions shown in **A**, relative to mitochondrial OCR of control cells ($N = 6$). **C**: Total OCR was measured in cells infected for 144 hours with control or siEXOG adenovirus ($N = 6$). **D**: Quantification of mitochondrial OCR (Mito), maximal OCR (Max.), reserve capacity (Res.Cap.) and ATP-linked OCR (ATP) of the conditions shown in **C**, relative to mitochondrial OCR of control cells ($N = 6$). OCR was corrected for total protein levels in each well, and all measurements were performed at least in triplicates. All graphs depict means and SEM; independent-samples t-test was performed to compare the difference between both groups. #$p < 0.05$ as compared with control with PE. EXOG silencing is indicated as siEXOG.

against cleaved caspase 3, which is the activated form of caspase 3, and this is a well-known marker for apoptosis. This did not show an increase in apoptotic cells under the different conditions (Fig. 6A and B). Western blotting revealed, however, a faint cleaved caspase 3 band after overexposure of the blot, but this was not different between control and EXOG-depleted cells (Supporting Information Figure 3). No specific increase of cleaved caspase 3 in EXOG-depleted cells was observed. Also, Terminal deoxynucleotidyl transferase dUTP nick end labeling (TUNEL) staining was performed, and positive nuclei could be detected in the NRVC cultures, but these were always devoid of cytoplasmic staining (Supporting Information Figure 4). This is suggestive of nuclear remnants of dead cells and not of early apoptotic cells. Also, late necrotic cells become TUNEL cardiomyocytes and become TUNEL positive [25]. NRVCs could be detected in the EXOG PE-treated cultures that showed abnormal shrinkage and are probably dying cells, but these were always TUNEL negative (Supporting Information Figure 4A). Cells were also treated with the pan caspase inhibitor Z-VAD fmk

(20 μM). Treatment of the cells with this inhibitor did not affect the cells after 72 hours of EXOG depletion. Moreover, Z-VAD fmk did not inhibit EXOG depletion-induced cell death after 144 hours (Fig. 6C and D). All together, these data suggest that apoptosis is not a major driver of cell death in EXOG-depleted cells.

As ROS production was increased in EXOG-depleted cells, we treated the cells with the ROS scavenger MitoTEMPO as high ROS levels also might induce cell death. As shown in Fig. 6E and F, MitoTEMPO had no effect on the EXOG-depleted cells after 72 hours of silencing and also did not prevent prolonged EXOG depletion-induced cell death.

Another major cell death mechanism in cardiomyocytes is necrosis. Necrotic cell death is characterized by loss of cytoplasmic content, and the presence of extracellular LDH activity is a clear sign of necrosis [26]. LDH activity significantly increased after prolonged depletion of EXOG, and the activity was further increased in combination with PE (Fig. 6G and H). This suggests that prolonged EXOG depletion caused necrosis, and, again, this was strongly augmented by PE.
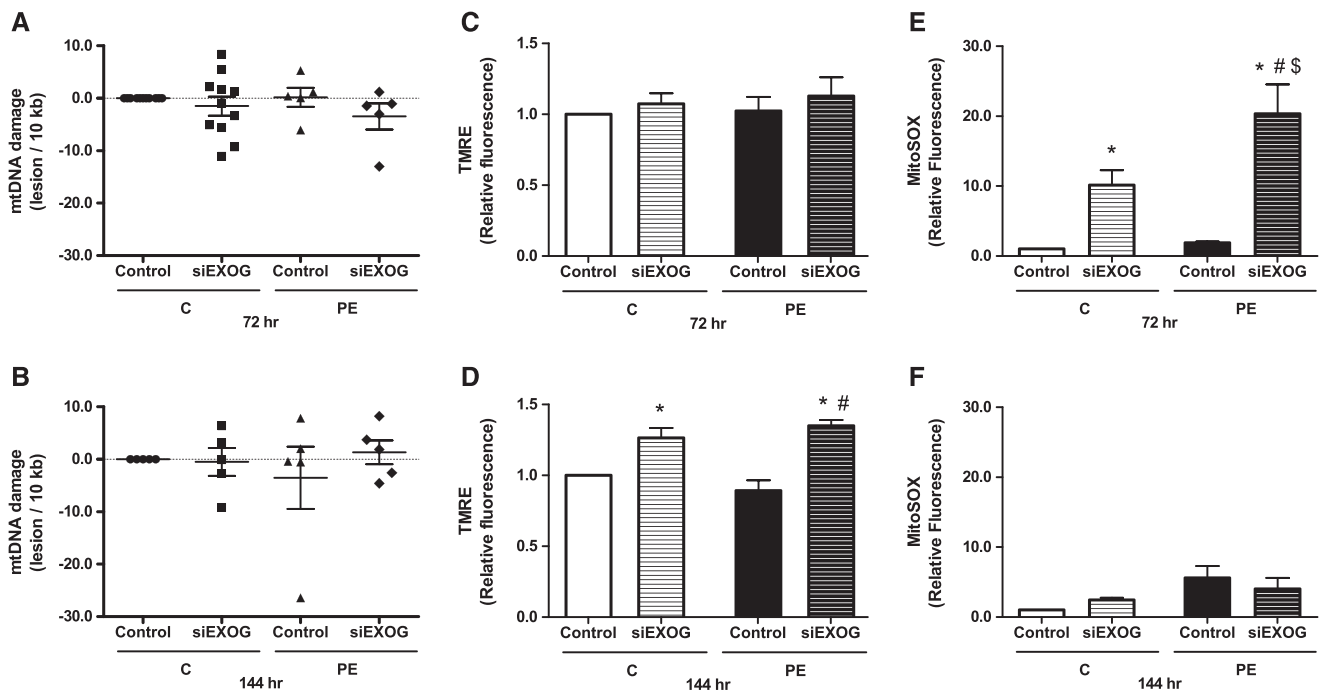
Figure 4. Effect of EXOG depletion on mtDNA damage, mitochondrial membrane potential and ROS production. Cells were stimulated with or without PE and infected with control or EXOG silencing adenovirus (siEXOG) for the indicated time. **A** and **B**: Mitochondrial DNA damage was measured using RT-PCR after 72 hours silencing (**A**) or 144 hours (**B**) ($N = 5$–11). **C** and **D**: Mitochondrial membrane potential was measured using TMRE after 72 hours silencing (**C**) or 144 hours (**D**) ($N = 4$–6). **E** and **F**: Mitochondrial superoxide production was measured using MitoSOX after 72 hours silencing (**E**) or 144 hours (**F**) ($N = 10$–14). Fluorescence was measured in quadruplicates per experiment. All graphs depict means and SEM; a one-way ANOVA with post hoc Bonferroni test was used to compare the difference between multiple groups. *$p < 0.05$ as compared with control; #$p < 0.05$ as compared with control with PE; \$$p < 0.05$ as compared with siEXOG.
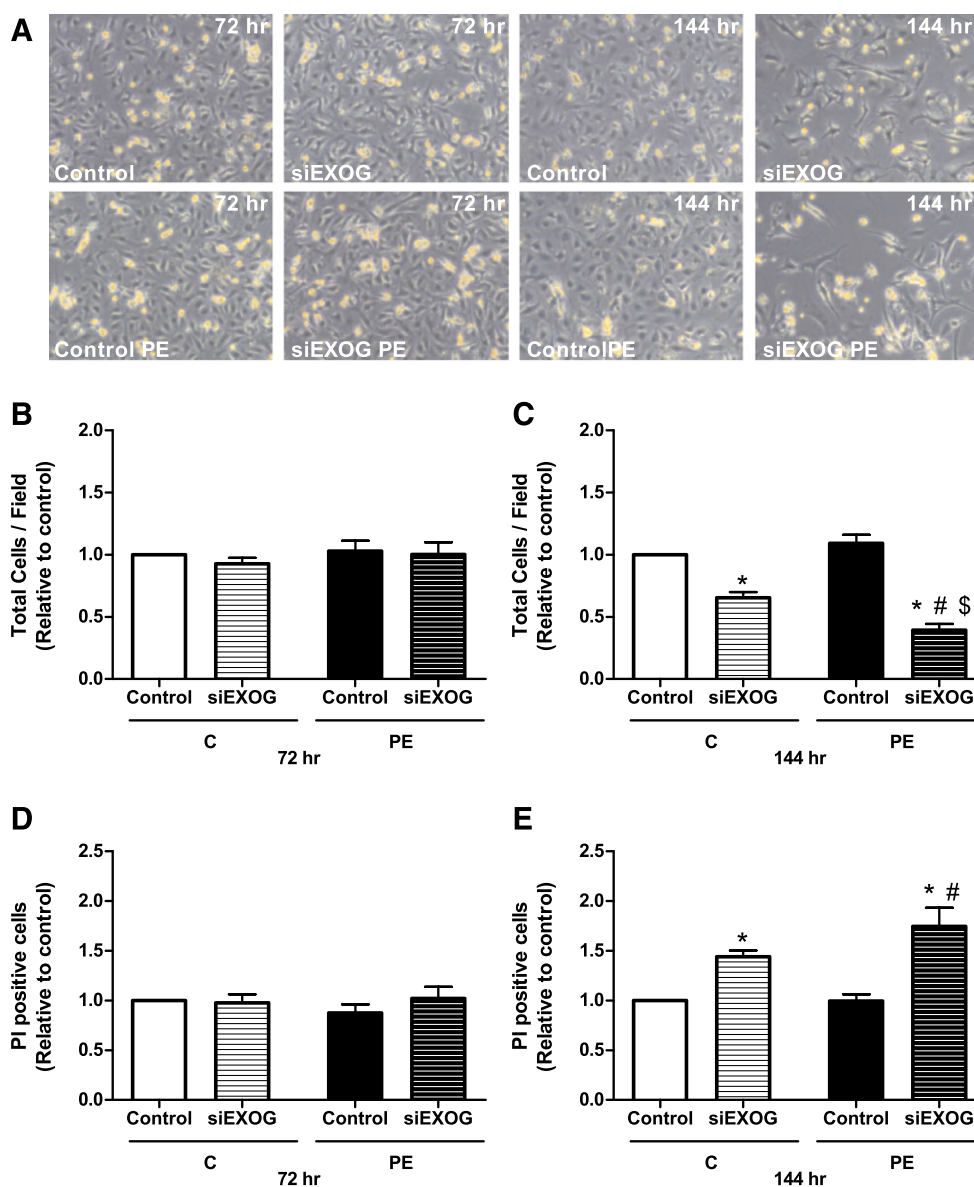
Discussion

In this study, we show that EXOG is an important gene in cardiomyocytes and that cell death is enhanced in EXOG-depleted cells treated with the pathological stress factor PE. We have recently shown that EXOG depletion activated mitochondrial respiration and induced ROS-mediated hypertrophy [14]. We confirmed these findings here but now also investigated the effects of prolonged EXOG depletion and the effects of EXOG depletion under pathological stress conditions. These results show that EXOG is important to maintain homeostasis in cardiomyocytes, but this is not related to its purported function in maintaining mtDNA integrity. EXOG depletion first resulted in improved mitochondrial respiration, but in time, and particularly after PE stimulation, mitochondrial respiration declined. Interestingly, diminished maximal respiration and reserve capacity were the first signs of mitochondrial dysfunction in these cells resulting in cellular death. Although we do not know the mechanisms underlying these changes, it is highly interesting that depletion of EXOG first stimulates mitochondrial function and cell growth but, in the long run, results in mitochondrial dysfunction and cell death.

Initially, mitochondrial respiration in EXOG-depleted cells was increased, but prolonged depletion resulted in a decrease in respiration, and this is more pronounced in the presence of PE. The decline in maximal respiration and reserve capacity was the first sign that mitochondrial respiration was hampered in EXOG-depleted cells stimulated with PE, which ultimately resulted in cell death. Previously, the metabolic reserve capacity was shown to be important for maintaining cellular function during acute and chronic stress [23]. In endothelial cells, the exhaustion of the reserve capacity by ROS leads to mitochondrial protein modifications, ultimately resulting in cell death [27, 28]. As the ROS scavenger MitoTEMPO did not prevent cell death in EXOG-depleted cardiomyocytes, it appears unlikely that the initial higher levels of ROS are responsible for cell death under these conditions. As EXOG depletion-induced ROS production could not be decreased by treatment with MitoTEMPO, we suggest that increased ROS levels are implicated in several other effects on the cell, including cardiac hypertrophy [14]. Apparently, this is a more direct effect of EXOG on mitochondrial function and maintaining reserve capacity. Although reserve capacity is still a vague term and its exact role is not clear, it probably provides cells with the flexibility to adapt to changing conditions. Our result that diminishment of reserve capacity in EXOG-depleted cells is the first sign in a process leading to cell death underscores the importance of the reserve capacity. It will therefore be very interesting to investigate whether a decline in reserve capacity is in general a first sign that marks subsequent cell death.

Cell death in EXOG-depleted cells did not appear to be an effect of enhanced stress levels. On the contrary, expression of the cardiac stress marker ANP did not significantly change in EXOG-depleted cells and was even diminished in EXOG-depleted cells in the presence of PE as compared with control PE-treated cells. Also oxidative stress markers (catalase and MnSOD) were

Figure 5. Effect of EXOG depletion on cell death. Cells were stimulated with or without PE and infected with control or EXOG silencing adenovirus (siEXOG) for the indicated time. **A**: Representative images of control and EXOG-depleted cells with and without PE. **B** and **C**: Cells were stained with Hoechst, and total cells per field were counted after 72 hours (**B**) or 144 hours (**C**) silencing. For quantification, at least 150 cells were counted per experiment ($N = 6$–8). **D** and **E**: Cells were stained with propidium iodide (PI) and counterstained with Hoechst. PI-positive cells were counted and corrected for total cells per field after 72 hours of silencing (**D**) or 144 hours (**E**) ($N = 6$). All graphs depict means and SEM; a one-way ANOVA with post hoc Bonferroni test was used to compare the difference between multiple groups. *$p < 0.05$ as compared with control; #$p < 0.05$ as compared with control with PE; $$p < 0.05$ as compared with siEXOG.

notincreased in EXOG-depleted cells [14]. Although we cannot rigorously exclude activation of other stress markers, it may indicate that there is no increased stress level in these cells. However, as an alternative hypothesis, EXOG depletion may also prevent activation of protective stress responsive pathways and consequently drives cells into cell death under stress conditions. ANP has cardiomyocyte protective actions via cGMP-mediated signaling [29], but its expression is repressed in EXOG-depleted cells. Although it will be difficult to discriminate between these two possibilities, further investigation of how EXOG may affect stress levels or stress protection will be highly relevant.

A multitude of mitochondrial alterations is observed in a temporal manner in EXOG-depleted cells, and these can be enhanced by PE stimulation. Whereas depletion of EXOG first stimulates mitochondrial OCR, in time, a decline is observed. ROS production is first increased but normalizes later, whereas mitochondrial potential is first comparable with control cells but increases at later stages. These pleiotropic responses make it very difficult to determine the direct effects of EXOG, and most mitochondrial processes are strongly interlinked. The mitochondrial membrane potential ($\Delta\psi$), for example, controls ATP synthesis, generation of ROS, mitochondrial
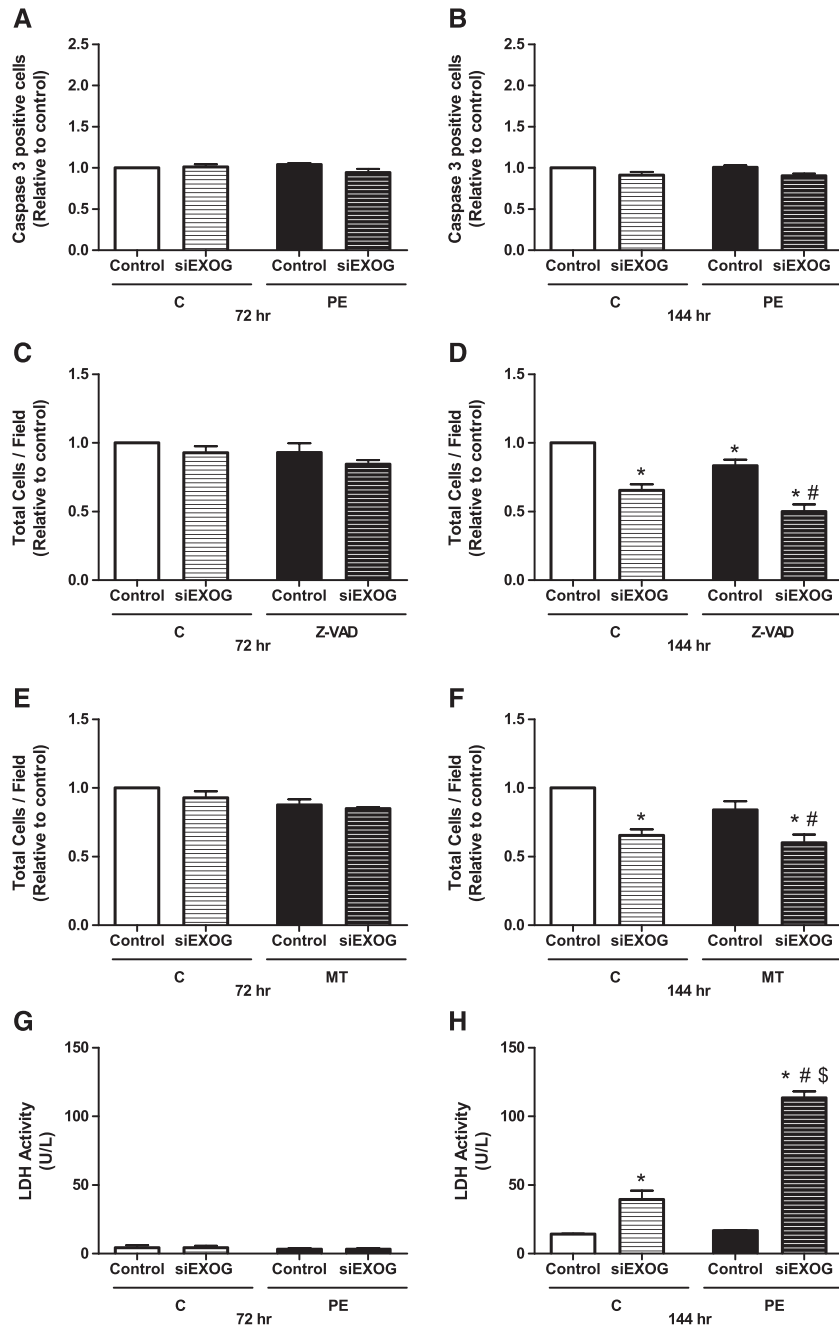
Figure 6. EXOG depletion results in cell death via necrosis. **A** and **B**: Cells were stained with specific cleaved caspase 3 antibody, and positive cells were counted after 72 hours of silencing (**A**) or 144 hours (**B**) ($N = 6$–8). **C** and **D**: Cells were treated with the pan caspase inhibitor Z-VAD fmk, cells were stained with Hoechst and total cells per field were counted after 72 hours of silencing (**C**) or 144 hours (**D**) ($N = 4$–8). **E** and **F**: Cells were treated with the ROS scavenger MitoTEMPO, cells were stained with Hoechst and total cells per field were counted after 72 hours silencing (**E**) or 144 hours (**F**) ($N = 4$–8). **G** and **H**: LDH activity was measured in cell culture medium after 72 hours of silencing (**G**) or 144 hours (**H**) ($N = 4$–6). All graphs depict means and SEM; a one-way ANOVA with post hoc Bonferroni test was used to compare the difference between multiple groups. *$p < 0.05$ as compared with control; #$p < 0.05$ as compared with control with PE; $$p < 0.05$ as compared with siEXOG. EXOG silencing is indicated as siEXOG.

calcium sequestration, import of proteins into the mitochondrion and mitochondrial membrane dynamics [30, 31]. Conversely, $\Delta\psi$ is controlled by ATP utilization, mitochondrial proton conductance, respiratory chain capacity and mitochondrial calcium [31, 32]. So, it is difficult to interpret the single

events, and the increased $\Delta\psi$ observed at later time points could be a result of many different factors. This high $\Delta\psi$ is, however, in agreement with the absence of apoptosis, which is accompanied by MPTP opening and consequently a decreased $\Delta\psi$.

All together, our results show that in neonatal cardiomyocytes, loss of EXOG initially enhances mitochondrial function and induces cell growth, but in time, mitochondrial function declines. This is not a result of mtDNA damage or induction of apoptosis but a result of mitochondrial dysfunction resulting in cell death, which can be enhanced by pathological stimulation. Most interestingly, a decline in mitochondrial reserve capacity is the first sign of mitochondrial dysfunction under these conditions.

Acknowledgements

References

1. **Frey N**, **Olson EN**. 2003. Cardiac hypertrophy: the good, the bad, and the ugly. *Annu Rev Physiol* **65**: 45–79.
2. **Kehat I**, **Molkentin JD**. 2010. Molecular pathways underlying cardiac remodeling during pathophysiological stimulation. *Circulation* **122**: 2727–35.
3. **Maillet M**, **van Berlo JH**, **Molkentin JD**. 2013. Molecular basis of physiological heart growth: fundamental concepts and new players. *Nat Rev Mol Cell Biol* **14**: 38–48.
4. **Bernardo BC**, **Weeks KL**, **Pretorius L**, **McMullen JR**. 2010. Molecular distinction between physiological and pathological cardiac hypertrophy: experimental findings and therapeutic strategies. *Pharmacol Ther* **128**: 191–227.
5. **Van Berlo JH**, **Maillet M**, **Molkentin JD**. 2013. Signaling effectors underlying pathologic growth and remodeling of the heart. *J Clin Invest* **123**: 37–45.
6. **Massie BM**, **Schaefer S**, **Garcia J**, **McKirnan MD**, et al. 1995. Myocardial high-energy phosphate and substrate metabolism in swine with moderate left ventricular hypertrophy. *Circulation* **91**: 1814–23.
7. **Osterholt M**, **Nguyen TD**, **Schwarzer M**, **Doenst T**. 2013. Alterations in mitochondrial function in cardiac hypertrophy and heart failure. *Heart Fail Rev* **18**: 645–56.
8. **Bayeva M**, **Gheorghiade M**, **Ardehali H**. 2013. Mitochondria as a therapeutic target in heart failure. *J Am Coll Cardiol* **61**: 599–610.
9. **Rosca MG**, **Tandler B**, **Hoppel CL**. 2013. Mitochondria in cardiac hypertrophy and heart failure. *J Mol Cell Cardiol* **55**: 31–41.
10. **Ardehali H**, **Sabbah HN**, **Burke MA**, **Sarma S**, et al. 2012. Targeting myocardial substrate metabolism in heart failure: potential for new therapies. *Eur J Heart Fail* **14**: 120–9.
11. **Tsutsui H**, **Kinugawa S**, **Matsushima S**. 2009. Mitochondrial oxidative stress and dysfunction in myocardial remodelling. *Cardiovasc Res* **81**: 449–56.
12. **Galluzzi L**, **Kepp O**, **Trojel-Hansen C**, **Kroemer G**. 2012. Mitochondrial control of cellular life, stress, and death. *Circ Res* **111**: 1198–207.
13. **Tait SWG**, **Ichim G**, **Green DR**. 2014. Die another way – non-apoptotic mechanisms of cell death. *J Cell Sci* **127**: 2135–44.
14. **Tigchelaar W**, **Yu H**, **De Jong AM**, **van Gilst WH**, et al. 2015. Loss of mitochondrial exo/endonuclease EXOG affects mitochondrial respiration and induces ROS mediated cardiomyocyte hypertrophy. *Am J Physiol Cell Physiol* **308**: C155–C163 ajpcell.00227.2014.
15. **Sotoodehnia N**, **Isaacs A**, **de Bakker PIW**, **Dörr M**, et al. 2010. Common variants in 22 loci are associated with QRS duration and cardiac ventricular conduction. *Nat Genet* **42**: 1068–76.
16. **Tann AW**, **Boldogh I**, **Meiss G**, **Qian W**, et al. 2011. Apoptosis induced by persistent single-strand breaks in mitochondrial genome: critical role of EXOG (5′-EXO/endonuclease) in their repair. *J Biol Chem* **286**: 31975–83.
17. **Szczesny B**, **Olah G**, **Walker DK**, **Volpi E**, et al. 2013. Deficiency in repair of the mitochondrial genome sensitizes proliferating myoblasts to oxidative damage. *PLoS One* **8**: 1–13 e75201.
18. **Lu B**, **Yu H**, **Zwartbol M**, **Ruifrok WP**, et al. 2012. Identification of hypertrophy- and heart failure-associated genes by combining in vitro and in vivo models. *Physiol Genomics* **44**: 443–54.
19. **Lu B**, **Tigchelaar W**, **Ruifrok WP**, **Van Gilst WH**, et al. 2012. DHRS7c, a novel cardiomyocyte-expressed gene that is down-regulated by adrenergic stimulation and in heart failure. *Eur J Heart Fail* **14**: 5–13.
20. **Yu H**, **Tigchelaar W**, **Lu B**, **van Gilst WH**, et al. 2013. AKIP1, a cardiac hypertrophy induced protein that stimulates cardiomyocyte growth via the Akt pathway. *Int J Mol Sci* **14**: 21378–93.
21. **Yu H**, **Tigchelaar W**, **Koonen DPY**, **Patel HH**, et al. 2013. AKIP1 expression modulates mitochondrial function in rat neonatal cardiomyocytes. *PLoS One* **8**: 1–11 e80815.
22. **Rothfuss O**, **Gasser T**, **Patenge N**. 2010. Analysis of differential DNA damage in the mitochondrial genome employing a semi-long run real-time PCR approach. *Nucleic Acids Res* **38**: 1–10 e24.
23. **Sansbury B**, **Jones S**, **Riggs DW**, **Darley-Usmar VM**, et al. 2011. Bioenergetic function in cardiovascular cells: the importance of the reserve capacity and its biological regulation. *Chem Biol Interact* **191**: 288–95.
24. **Hill BG**, **Dranka BP**, **Zou L**, **Chatham JC**, et al. 2009. Importance of the bioenergetic reserve capacity in response to cardiomyocyte stress induced by 4-hydroxynonenal. *Biochem J* **424**: 99–107.
25. **De Jong AM**, **Maass AH**, **Oberdorf-Maass SU**, **De Boer R a**, et al. 2013. Cyclical stretch induces structural changes in atrial myocytes. *J Cell Mol Med* **17**: 743–53.
26. **Chan FKM**, **Moriwaki K**, **De Rosa MJ**. 2013. Detection of necrosis by release of lactate dehydrogenase (LDH) activity. *Methods Mol Biol* **979**: 65–70.
27. **Módis K**, **Gero D**, **Erdélyi K**, **Szoleczky P**, et al. 2012. Cellular bioenergetics is regulated by PARP1 under resting conditions and during oxidative stress. *Biochem Pharmacol* **83**: 633–43.
28. **Dranka BP**, **Benavides GA**, **Diers AR**, **Giordano S**, et al. 2011. Assessing bioenergetic function in response to oxidative stress by metabolic profiling. *Free Radic Biol Med* **51**: 1621–35.
29. **Kato T**, **Muraski J**, **Chen Y**, **Tsujita Y**, et al. 2005. Atrial natriuretic peptide promotes cardiomyocyte survival by cGMP-dependent nuclear accumulation of zyxin and Akt. *J Clin Invest* **115**: 2716–30.
30. **Baines CP**. 2010. The cardiac mitochondrion: nexus of stress. *Annu Rev Physiol* **72**: 61–80.
31. **Skárka L**, **Ostádal B**. 2002. Mitochondrial membrane potential in cardiac myocytes. *Physiol Res* **51**: 425–34.
32. **Perry SW**, **Norman JP**, **Barbieri J**, **Brown EB**, et al. 2011. Mitochondrial membrane potential probes and the proton gradient: a practical usage guide. *Biotechniques* **50**: 98–115.

Supporting information

Additional supporting information may be found in the online version of this article at the publisher's web site.